Available online at www.sciencedirect.com
SCIENCE DIRECT®
Applied Catalysis A: General 253 (2003) 337–358
APPLIED CATALYSIS A: GENERAL
www.elsevier.com/locate/apcata

Review

Carbon nanotubes and nanofibers in catalysis

Philippe Serp*, Massimiliano Corrias, Philippe Kalck

Laboratoire de Catalyse, Chimie Fine et Polymères, Ecole Nationale Supérieure d'Ingénieurs en Arts Chimiques Et Technologiques, 118 Route de Narbonne Toulouse Cedex 31077, France

Received 5 February 2003; received in revised form 30 June 2003; accepted 30 June 2003

Abstract

This review analyses the literature from the early 1990s until the beginning of 2003 and covers the use of carbon nanotubes (CNT) and nanofibers as catalysts and catalysts supports. The article is composed of three sections, the first one explains why these materials can be suitable for these applications, the second describes the different preparation methods for supporting metallic catalysts on these supports, and the last one details the catalytic results obtained with nanotubes or nanofibers based catalysts. When possible, the results were compared to those obtained on classical carbonaceous supports and explanations are proposed to clarify the different behaviors observed.

Keywords: Carbon nanotubes; Graphite nanofibers; Catalyst support; Catalyst preparation

1. Introduction

Among the different types of supports used in heterogeneous catalysis carbon materials attract a growing interest due to their specific characteristics which are mainly: (i) resistance to acid/basic media, (ii) possibility to control, up to certain limits, the porosity and surface chemistry and (iii) easy recovery of precious metals by support burning resulting in a low environmental impact. Several reviews dealing with this subject have been published [1–3]. Recently, new carbon forms like graphite nanofibers (GNF) or nanofilaments and carbon nanotubes (CNT) have generated an intense effervescence in the scientific community. However, it has got to be remembered that carbon nanofilaments have been synthesized for very long as products from the action of a catalyst over the gaseous species originating from the thermal decomposition of hydrocarbons. One of the first evidence that the nanofilaments thus produced could have been nanotubes, exhibiting an inner cavity, can be found in the transmission electron microscope micrographs published by Hillert and Lange [4]. The production of graphite nanofibers is even older and the first reports date of more than a century [5,6]. The interest in fibrous carbon has since then been recurrent and a significant boost in the research in carbon nanostructure field coincides with the discovery of multi-wall carbon nanotubes (MWNT) by Iijima [7] and the successive production of single-wall nanotubes (SWNT) [8,9]. CNT have since then become one of the most active fields of nanoscience and nanotechnology due to their exceptional properties that make them suitable for many potential applications as polymer reinforcements for composites or breakthrough materials for energy storage, electronics and catalysis. Of course, such a promising material attracts the interest of industrial groups that foresee a high economical impact

* Corresponding author. Tel.: +33-562-8857-00; fax: +33-562-8856-00.
E-mail address: Philippe.Serp@ensiacet.fr (P. Serp).

0926-860X/$ – see front matter © 2003 Elsevier B.V. All rights reserved.
doi:10.1016/S0926-860X(03)00549-0

in the near future. Indeed, a bibliometric analysis has shown that there is a considerable thrust on patenting in the area of synthesis or processes for the production of CNT, mainly in the USA and Japan, and to a lesser extent in Europe or Korea [10]. Currently, one of the main challenges is the low cost, industrial scale production of nanotubes that might be achieved by exploiting chemical vapor deposition (CVD) processes. A major industrial group (Mitsui & Co. Ltd.) as well as some SME's (Hyperion Catalysis, Nanotech, ...) and several start-up companies (Nanoledge, Nanocyl, Rosseter, ...) are involved in CNT synthesis, but the whole worldwide annual production should not exceed some hundreds of kilograms of MWNT and some kilos of SWNT. Up to date, no precise price estimations nor anticipations are possible since no market price has been fixed, but middle term scenorii predict a price that could vary between 15 and 50 €/kg for MWNT, and between 50 and 100 €/kg for SWNT.

Among the main possible applications we will concentrate, in this article, on the use of CNT or GNF in the field of catalysis; indeed, the potentiality of using these new materials as catalyst supports has already been investigated and preliminary results have been already reviewed [11–13]. Here also, an industrial interest exists in the area of fuel cells electrodes [14] or supported catalysts for fluid phase reactions [15]. We will analyzed successively the main characteristics of CNT and GNF, the preparation routes to supported catalysts on CNT or GNF and finally the catalytic studies performed on such systems.

2. Why CNT or GNF may be suitable to be used as catalyst supports?

Before presenting a detailed description of the use of carbon nanotubes and nanofibers as efficient catalysts or catalyst supports, it is important to analyze their electronic, adsorption, mechanical and thermal properties. It is indeed necessary to evaluate the resistance of this type of material and to be able to foresee how the metallic particles will be anchored on the support and how the reagents would interact with the catalyst, so as to understand what such novel carbon forms could bring to catalysis. Thus, a first overview will be dedicated to analyze those properties with respect to catalytic requirements.

2.1. Structural features

First of all, we will recall briefly the structural features of nanotubes and nanofibers. Carbon nanotubes can be divided essentially into two categories: SWNT and MWNT as displayed in Fig. 1. Ideally, single-wall carbon nanotube are made of a perfect graphene sheet, i.e. a polyaromatic mono-atomic layer made of an hexagonal display of sp^2 hybridized carbon atoms that genuine graphite is built up with, rolled up into a cylinder and closed by two caps (semi-fullerenes). The internal diameter of these structures can vary between 0.4 and 2.5 nm and the length ranges from few microns to several millimetres. MWNT can be considered as concentric SWNT with increasing diameter and coaxially disposed. The number of walls present can vary from two (double wall nanotubes) to several tens, so that the external diameter can reach 100 nm. The concentric walls are regularly spaced by 0.34 nm similar to the intergraphene distance evidenced in turbostratic graphite materials. It is worth to note that residual metallic particles coming from the production process can be found in the inner cavity of MWNT (see Fig. 1). The main difference between nanotubes and nanofibers consists in the lack of an hollow cavity for the latter. In this review, we will mainly concentrate on three types of GNF which differ for the disposition of the graphene layers: in ribbon-like GNF (GNF-R) the graphene layers are parallel to the growth axis, the platelet GNF (GNF-P) display graphene layers perpendicular to the growth axis and finally herringbone nanofibers have layers stacked obliquely in respect to the growth axis (see Fig. 1). The diameters of GNF are generally higher than the ones presented by nanotubes and can easily reach 500 nm.

2.2. Electronic properties

Exhaustive studies concerning electronic properties of both SWNT [16] and MWNT [17], are available in the literature, whereas GNF are often considered as conductive substrates that can exert electronic perturbations similar to those of graphite [18].

In the case of SWNT, studies have demonstrated that they behave like pure quantum wires (1D-system) where the electrons are confined along the tube axis. Electronic properties are mainly governed by two factors: the tube diameter and the helicity, which is

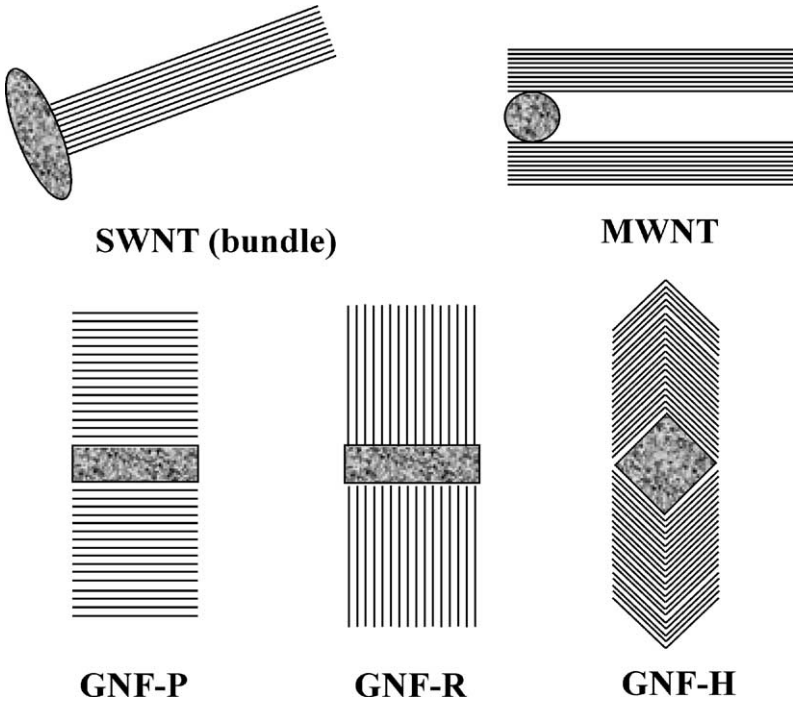

Fig. 1. Different types of CNT and GNF.

defined by the way in which the graphene layer is rolled up [19] (armchair, zigzag or chiral). In particular, armchair SWNT are metallic and zigzag ones display a semi-conductor behavior. This curvature of the graphene sheet induces strong modifications of the electronic properties and a comparison to graphite shows a modification of the π-electron cloud [20,21]. It is however worth to note that these theoretically predicted electronic properties are often drastically modified by the presence of defects such as pentagons, heptagons, vacancies or impurities [22]. In addition, production techniques do not currently allow a selective production of one specific type of SWNT and the final purity of the obtained material, i.e. after purification steps, is far from being perfect.

Studies on MWNT's electronic properties have revealed that they behave like an ultimate carbon fiber [17]: at high temperature their electrical conductivity may be described by semi-classical models already used for graphite, whereas at low temperature they reveal 2D-quantum transport features. A fine prediction of the electronic properties is even more difficult than in the case of SWNT due to two main factors: the rolling up of the graphene layers can vary along the different walls of a single MWNT and the higher complexity of the structure will increase the possibility of the presence of defects.

When used in catalysis, these conductive supports present clear differences with respect to activated carbon, and a recent theoretical study related to the interaction of transition metal atoms with CNT and graphite indicates major differences [23]. It has been demonstrated that the binding sites are depending on the structure of the support: the studies conducted over nickel show that the most stable anchoring sites vary sensibly between graphite and SWNT due to the different curvature of the surfaces where the active species can be deposited. The curvature also affects significantly the values of magnetic moments on the nickel atoms on the nanotube's wall and the charge transfer direction between nickel and carbon can be inverted. Therefore, the possibility of peculiar metal–support interaction has to be taken into account.

2.3. Adsorption properties

The interaction of carbon nanotubes with their environment, and in particular with gases or doping species adsorbed either on their internal or external surfaces attracts increasing attention due to the possible influence of the adsorption on some of the tubes properties and to the possibility of using these materials for efficient gas storage. Adsorption properties on SWNT samples, usually found in bundles or ropes, should not be considered in terms of individual nanotubes but in term of adsorption on the exterior or interior surfaces of such bundles. A similar situation exists for MWNT where adsorption could occur either on or inside the tube or between aggregated MWNT. Additionally, it has been shown that the curvature of the graphene sheets can results in a lower heat of adsorption with respect to this on a planar graphitic surface. Indeed, the rolling up of the graphene sheet to form the tube causes a rehybridization of carbon orbital (non-planar sp^2 configuration), thus leading to modifications of the π-density of the graphene sheet.

Different studies dealing with the adsorption of nitrogen on MWNT [24,25] and SWNT [26] have highlighted the porous nature of these materials. Pores in MWNT can be mainly divided into inner hollow cavities of small diameter (narrowly distributed, mainly 3–6 nm) and aggregated pores (widely distributed, 20–40 nm) formed by interaction of isolated MWNT, the latter being much more important for adsorption. On as-prepared and acid-treated SWNT, adsorption of N_2 has clearly evidenced the microporous nature of SWNT samples, contrarily to the MWNT mesoporous nature. Experimentally, the specific surface area of SWNT is often larger than that of MWNT. Typically, total surface area of as-grown SWNT ranged between 400 and 900 $m^2\,g^{-1}$ (micropore volume, 0.15–0.3 $ml\,g^{-1}$) whereas, for as-produced MWNT values ranging between 200 and 400 $m^2\,g^{-1}$ are often reported. In the case of SWNT, the diameter of the tubes and the number of tubes in the bundle will affect mainly the BET value. Worthy to note is that opening/closure of the central canal noticeably affects the adsorptive properties of nano-tubes. For GNF, the surface area can range from 10 to 200 $m^2\,g^{-1}$, no micropores are found and the mesopore volume ranges between 0.5 and 2 $ml\,g^{-1}$ [13].

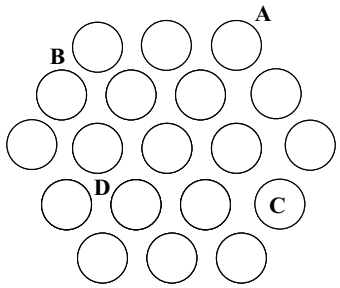

Fig. 2. Different adsorption sites in SWNT bundles: (A) surface; (B) groove; (C) pores; (D) interstitial.

Adsorption sites in a SWNT bundle can be either the inside of the tubes (pore), the interstitial triangular channels between the tubes, the outer surface of the bundle or the grooves formed at the contact between adjacent tubes on the outside of the bundle (see Fig. 2). For MWNTs, adsorption can occur in the aggregated pores, inside the tube or on the external walls, in this latter case the presence of defects, as incomplete graphene layers, has to be taken into consideration. Although adsorption between the walls has been proposed in the case of hydrogen adsorption in herringbone type graphite nanofibers [27], it is unlikely to occur in the case of MWNT due, for many molecules, to steric effect and should not prevail for small molecules due to long diffusion paths.

Few studies deal with adsorption sites in MWNT. However, it has been shown that, in the case of butane, MWNT with smaller outside diameters sorbed more butane, consistently with other findings that the strain in curved graphitic surfaces affects sorption. Most of the butane sorbed on the external surface of the MWNT and only a small fraction of the gas condensed in the pores [28]. Higher condensation pressure and lower heat of adsorption were found on nanotubes with respect to graphite [29]. These differences mainly result from a decrease in the lateral interactions between the adsorbed molecules, in direct relationship with the curvature of the graphene sheets.

The observed trends in the binding energies of gases with different van der Walls radii suggest that the groove sites of SWNT are the preferred low coverage adsorption sites due to their higher binding energies. Furthermore several studies have shown that,

at low coverage, the binding energy of the adsorbate on SWNT is between 25 and 75% higher than the monolayer binding energy on graphite. The observed change of the binding energy can be attributed to an increase of the effective coordination in binding sites, as the groove sites, in SWNT bundles [30,31].

In summary, it appears that carbon nanotubes present specific adsorption properties when compared to graphite or to activated carbon, mainly due to their peculiar morphology, the role of defects, opening/closing of the tubes, chemical purification or the presence of impurities as catalyst particles that can govern the adsorption properties has not been yet examined in detail.

2.4. Mechanical and thermal properties

Nanotubes are made exclusively of covalently bonded carbon atoms and could therefore be, in theory, the most resistant fibers obtainable with a Young modulus of the order of the tera-Pascal [32] and a resistance to traction of 250 GPa [33] which would be one hundred times higher than the one displayed by steel while weighting six time less. In addition to these amazing resistance properties, it has been shown that CNT are flexible and can be bent several times at 90° without undergoing structural changes. Obviously, these values are theoretical and the presence of defects will reduce them, but their resistance will still be very high. The structure is not easily changed with the effects of pressure, and it has been demonstrated [34] that CNT are only undergoing permanent structure changing at very high pressures (over 1.5 GPa) and that below that value the deformations are totally elastic. We have also conducted some experiments to evaluate the behavior of MWNT under the effect of pressure and temperature (5.5 GPa, 800 °C) and our results show that, under these conditions, some structural modifications occur [35]. Interesting mechanical properties have also been reported for GNF and GNF granules [13]. Thus, we believe that such a support will display as good or even better properties than an activated carbon.

Another important feature that has to be taken into consideration is the thermal stability under reaction conditions. The most common and simple way to study the resistance of the carbonaceous material towards temperature is thermogravimetric analysis (TGA). An important property that has to be noticed is that CNT or GNF are more stable to oxidation than activated carbon (C^*) but more reactive than graphite. However, the presence of residual metal on or in the nanotubes that can catalyse carbon gasification may lower the temperature at which the maximum gasification rate occurs. Fig. 3 shows the comparison between MWNT, activated carbon and graphite. GNF present a high resistance to air oxidation and present a maximum gasification rate at around 900 °C (heating rate: 5 °C min^{-1} under air/argon mixture) [36]. In our hands, purified GNF samples (10% remaining metal), produced from ethylene on Fe/SiO_2 catalysts, present a maximum gasification rate at 650 °C (heating rate: 10 °C min^{-1} under air; see Fig. 3). The Studies conducted on carbon nanotubes have shown distinguishable behaviors for SWNT and MWNT: single-wall nanotubes which have less defects on their surfaces and are therefore more stable than multi-wall ones. In the case of highly purified SWNT (less than 1% of metal) the maximum gasification rate is located at around 800 °C (heating rate: 10 °C min^{-1} under air) [37]. For purified MWNT (97%, 3% metal) and under the same oxidation conditions we have measured a maximum gasification rate at around 650 °C (see Fig. 3). TGA on a 92.5% MWNT material (7.5% metal) oxidized at 1 °C min^{-1} under air has shown the value at around 550 °C [38]. It has to be noticed that whatever material is considered the reported values can be affected by the concentration of surface defects and/or the presence of remaining metal particles that can catalyze carbon gasification.

To conclude, it appears that he combination of these properties makes CNT attractive and competitive catalyst supports by comparison with activated carbons. Indeed, resistance to abrasion, dimensional and thermal stability and specific adsorption properties are important factors in the final activity and reproducibility of the catalytic system. In particular, they could replace activated carbons in liquid-phase reactions as long as the properties of activated carbons are still difficult to control and their microporosity has often slowed down catalysts development. Table 1 summarizes the main properties of CNT and GNF and compares them to the ones of activated carbon, graphite and high surface graphite.

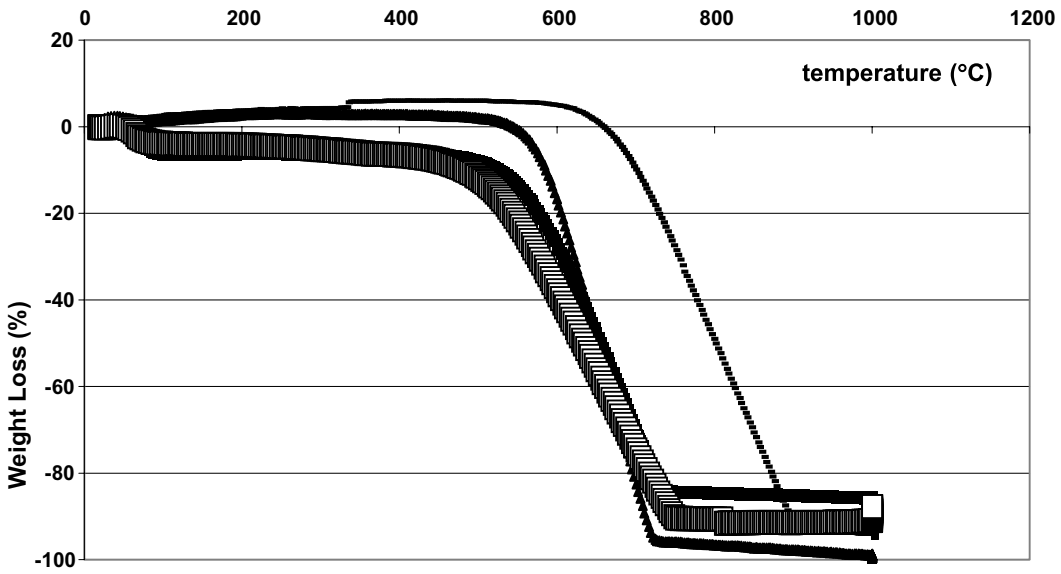

Fig. 3. Thermogravimetric analyses (20–1000 °C at 10 °C min^{-1} in air) of (▬) synthetic graphite, (▲) activated carbon, (□) GNF and (■) MWNT.

Table 1
Adsorption properties of CNT, GNF, activated carbon and graphite

Type of Carbon	Porosity (cm^3 g^{-1})	Surface area (m^2 g^{-1})	Thermal resistance in air atmosphere (°C)
SWNT	Microporous, V_{micro}: 0.15–0.3	400–900	~800
MWNT	Mesoporous, V_{meso}: 0.5–2	200–400	~650
GNF	Mesoporous, V_{meso}: 0.5–2	10–200	~600–900
Activated carbon	Microporous	700–1200	~500–600
HSAG	Mesoporous[a]	60–300	~800

[a] From agglomeration of small non-porous particles.

3. Different approaches for the anchoring of metal-containing species on CNT and GNF

Several methods such as incipient wetness impregnation, ion-exchange, organometallic grafting, electron beam evaporation and deposition/precipitation have been used to prepare carbon nanotubes or graphite nanofibers supported catalysts (see Table 2). As long as CNT and GNF are relatively inert supports many studies have been conducted in order to find which pre-treatment procedures are needed to achieve optimal interaction between the support and the catalyst precursor. In this section, we will analyze the different approaches for the anchoring of metal-containing species and classify them according to the pre-treatments steps that the supports may undergo, and a particular attention will be paid to the final dispersion of the metallic phase.

3.1. Deposition of metals on untreated supports

In the case of as-produced CNT it has to be noticed that such a material does not possess an high amount of functional groups on it's surface and mainly surface defects can be considered as anchoring sites for metals. For SWNT an interesting method to identify the location of surface chemical defects has been recently proposed [39] through the formation

Table 2
Representative examples of supported catalysts preparation

Metal/support (w/w)	Pre-treatment	Technique	Particle size (nm)	Reference
Ru/SWNT (0.2%)	None impure material	Impregnation from $[Ru(acac)_3]$–toluene solution	3.5	[42]
Pd/MWNT (9–44%)	None	Hydrogen reduction of $[Pd(hfacac)_2]$ in scc CO_2	5–10	[49]
Rh/GNF-R (4%)	None	Impregnation from $RhCl_3$ alcoholic solutions	15	[53]
Ir/GNF-graphite (30%)	None	Impregnation from H_2IrCl_6 solutions	2	[57]
Pt/MWNT (10%)	HNO_3–H_2SO_4	Impregnation from H_2PtCl_6 ethylene glycol solutions	2–4	[68]
Pt/SWNT (10%)	Nitric acid	Impregnation from $[K_2PtCl_4]$ ethylene glycol solutions	1–2	[61]
Rh/GNF-H (1%)	HNO_3–H_2SO_4	Ion-exchange from $RhCl_3$ aqueous solutions and $NaBH_4$ reduction	1–2	[75]
Rh/MWNT (1–10%)	Nitric acid + Na_2CO_3	Organometallic grafting from $[RhCl(CO)_2]_2$	1.5–5	[62]

of selenium nanoparticles via selective oxidation of absorbed H_2Se under mild conditions. This technique coupled with microscopy observations can reveal both location and density of the defects. Additionally, for high metal loadings and considering the tubular structure of CNT, the possibility of filling the tubes has to be taken into account [40]. Furthermore, in the case of SWNT bundles the intercalation of metal layers in the inter-tubular space has been reported [41].

Unpurified arc-produced nanotubes ($27\,m^2\,g^{-1}$) supports were used to prepare ruthenium catalysts from a toluene solution of $[Ru(acac)_3]$: the 0.2% (w/w) final material obtained after the decomposition and reduction under hydrogen presents a dispersion of 30% and a mean particle size of 3.5 nm [42]. The interaction between iron, cobalt or nickel and MWNT, SWNT, activated carbon or layered graphite has been studied in order to evaluate the role of surface defects on the final metal dispersion [43]. On SWNT and layered graphite, no coating was observed due to the low density of surface defects. For MWNT and activated carbon, a better wetting has been achieved and, in the case of iron on MWNT, a particle size of 5–15 nm has been measured. Several other metals were deposited on MWNT by using the wetness impregnation technique. Copper nanoparticles or nanowires were obtained by reaction between dispersed multi-walled nanotubes and a copper salt [44]. It is interesting to underline that, if the amount of copper salt is changed, a significant variation of the metal deposit can be observed: if the molar percentage of the metal precursor is lower than 1%, small particles (less than 10 nm) can be obtained whereas if the value is increased to 2% larger sizes (25–35 nm) were measured. A completely different type of structure was evidenced when using a 1:1 molar ratio between CNT and copper salt: a sponge-like material was obtained and SEM and TEM observations showed the formation of copper nanowires via coating of the CNT (100 nm to 5 μm of diameter). The same method was used to deposit other metals like palladium, platinum, silver and gold [45]. The reactions were conducted by dispersing MWNT with a diameter of roughly 20 nm in distilled water or acetone in an ultrasonic bath, adding a soluble metal salt (2% molar), heating until evaporation of the solvent and then reducing under hydrogen (300–700 °C, depending on the salt). The palladium, platinum, gold and silver particles obtained presented a mean size of 7, 8, 8 and 17 nm, respectively, and were mostly found on the outer surface of the CNT. The same reaction was realized using palladium and graphite or activated carbon: larger metallic particles were found emphasizing the unique template function of carbon nanotubes in tailoring the size of metal particles. Also with these metals it has been shown that by increasing the molar ratio between metal precursor and CNT larger particles are yielded. Metallic platinum and gold were also deposited on SWNT by spontaneous reduction of metal chloride ions in solution [46]. The obtained nanoparticles were measured to have a mean size of 7 nm for gold and 2 nm for platinum. The driving force that allows this spontaneous electron transfer from the SWNT to the metal ions and their reduction is the relative potential: indeed, for single-wall nano-tubes, the Fermi level is well above the reduction potentials of $AuCl_4^-$ and $PtCl_4^{2-}$. Electron beam evaporation was used to prepare metal nanowires or metal nanoparticles

on suspended SWNT and to study the metal–tube interaction [47,48]: several metals like gold, palladium, iron, aluminium, lead, nickel or titanium were deposited and the size of the resulting particles was measured by TEM. A substantially different behavior was evidenced according to the nature of the metal: indeed metals with weak interaction with the tube wall (gold, iron, aluminium, and lead) gave origin to dispersed nanoparticles of roughly 5 nm whereas palladium and nickel covered totally the support but still had a particle nature, whereas titanium formed a continuous nanowire structure. It is also worth to note that nanowires of different metals can be obtained by realizing the electron beam evaporation on already decorated nanotubes; thus, if the metal (gold, iron, aluminium or lead) is decomposed over SWNT covered by a 1 nm titanium coating that serves as a buffer level, a complete nanowire can be formed. Impregnation and hydrogen reduction of a palladium(II) β-diketone precursor in super-critical carbon dioxide has been reported to yield well dispersed (5–10 nm) palladium nanoparticles on MWNT even for high metal loadings (9–44%) [49].

Due to their peculiar structure, GNF are mainly used as catalytic supports without any pre-treatment, indeed platelets and herringbone structures present potentially reactive groups for metal anchoring. Extensive studies on nanofibers were conducted by the group of Baker in order to deposit metals by the wetness impregnation technique. Nickel was deposited on GNF with platelet or ribbon structure from $[Ni(NO_3)_2{\cdot}6H_2O]$ solutions [50,51]. A 5% (w/w) Ni/GNF material was compared with a similar activated carbon and γ-alumina supported catalysts. TEM observations show that the metal is evenly distributed on the GNF surface and that in general the particles adopted a well defined thin flat hexagonal shape. In contrast, the crystallites formed on the other supports did not display the same well defined morphology. Additionally, the particle size distribution varies strongly with the type of support and average particle sizes of 1.4 and 5.5 nm with sharp distributions were measured for γ-alumina and activated carbon, respectively, whereas on platelet or ribbon GNF, very broad particle size distribution (1–18 nm) centered at 8.1 nm is reported and has been recently confirmed by Otsuka et al. [52] who have measured a mean particle size ranging from 8 to 20 nm. A similar situation prevails for a 4% (w/w) rhodium supported on herringbone, platelet or ribbon GNF [53]. Indeed, rhodium crystallites located on the edges of herringbones GNF have an hexagonal shape, and independently on the type of nanofibers, large average particle sizes were measured with respect to rhodium supported on silica: Rh/GNF-R = 15.1 nm; Rh/GNF-H = 19.1 nm; Rh/GNF-P = 22.6 nm; Rh/SiO_2 = 2.6 nm. Surprisingly, the rhodium dispersion is not directly connected to the BET surface area of the GNF support: GNF-R = 51.5 $m^2\,g^{-1}$, Rh/GNF-R = 55.9 $m^2\,g^{-1}$ (15.1 nm) and GNF-H = 214.8 $m^2\,g^{-1}$, Rh/GNF-H = 212.4 $m^2\,g^{-1}$ (19.1 nm). In fact, a better dispersion on the herringbone fibers could have been expected thanks to their higher surface area and to the presence of potentially active graphene edges. Platinum was deposited on the three types of GNF by reaction with $[Pt(NH_3)_2(NO_2)_2]$ [19,54], the 5% (w/w) platinum on GNF-P [54] presenting a dispersion of 20%. Bimetallic iron–copper (7:3) catalytic systems were prepared from metallic salts on nanofibers (5% (w/w)) characterised by a BET surface area of 184 $m^2\,g^{-1}$ and compared with their homologues on activated carbon (517 $m^2\,g^{-1}$) or on γ-alumina (91 $m^2\,g^{-1}$). Here again the average metal particle size follows the order: alumina (5.3 nm) < activated carbon (7.8 nm) < GNF (12.4 nm, with broad distribution) [55]. A GNF supported platinum-ruthenium (1:1) catalytic system has also been prepared from an hetero-bimetallic complex in acetone solution [56]: on platelet or herringbone structures small particle sizes ranging between 4.8 and 8.6 nm were measured for high metal loadings (43–47% (w/w)). Graphite felt supporting 40 nm diameter carbon nanofibers was used as a support for high loaded iridium catalyst (30% (w/w)) prepared from H_2IrCl_6 solutions [57]. A narrow particle size distribution center at around 2 nm has been obtained, similar to the one observed on an alumina support; such a high dispersion has been attributed to the strong interaction between the iridium particles and the prismatic planes exposed by the nanofibers containing hydrophilic oxygenated surface groups.

3.2. Deposition of metals on surface modified supports

Like for classical carbon materials used in catalysis the possibility of chemical or thermal activation, in

order to modify the nature and concentration of surface functional groups, has been studied in the case of CNT and GNF. The influence of these treatments on the final dispersion of the metallic phase will be discussed in this section.

3.2.1. Nitric acid treatments

Among the different techniques that have been applied for the more or less pronounced surface oxidation, nitric acid treatments are the most common and it has been shown that surface oxygen functionalities like carboxylic groups can be introduced on the outer and possibly inner walls of the CNT [58,59], GNF-H or GNF-P [60].

For SWNT, a careful and slow oxidation step in diluted nitric acid is compulsory to create surface oxygenated groups, mostly carboxylic acid functions, and to minimize bulk damage to the material. With such a treatment, Lordi et al. have managed to obtain 1–2 nm platinum particles (10% (w/w)) from a [K_2PtCl_4] ethylene glycol solution [61]. In the case of MWNT, more drastic treatments can be performed: indeed the main significant structural modification occurs on the nanotubes tip and can result(s) in their opening (see Fig. 4), and the formation of edges and steps on the graphene sheets is possible [62]. Deposition of silver nanoparticles on nitric acid oxidized MWNT with a fairly narrow size distribution centered at 10 nm from aqueous silver nitrate solutions has been reported [63]. The same impregnation procedure was performed on untreated samples and has led to the formation of fewer nanoparticles due to the chemical inertness of the raw material. Other reactions from tin chloride acidic solutions have yielded extremely small nanoparticles located only on the surface of the oxidized tubes. Cobalt was deposited on raw and oxidized MWNT from a cobalt nitrate aqueous solution; after oxidation and reduction steps the nanoparticles presented a much smaller size and an higher dispersion on the treated support [64].

Cerium chloride solutions were reacted with nitric acid-treated MWNT in order to obtain nanosized (6 nm) ceria particles, here again the critical factor to well dispersed nanoparticles is the oxidation step [65]. Gold, platinum or silver clusters have been deposited on nitric acid-treated MWNT by ethylene glycol solutions impregnation or by refluxing the nanotubes with the metallic compounds and nitric

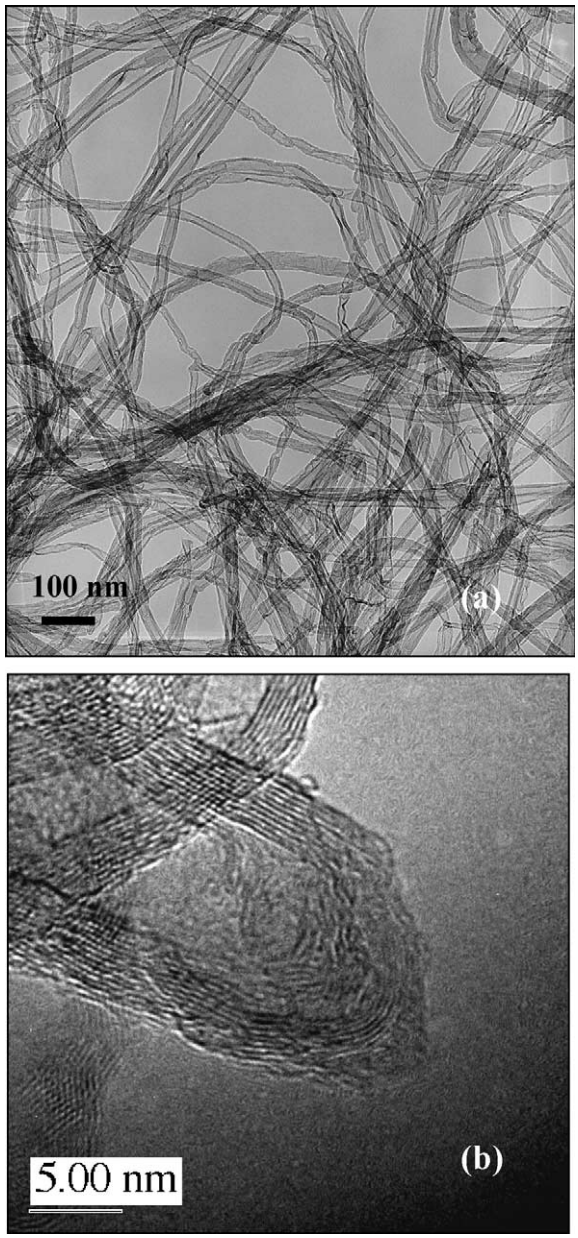

Fig. 4. TEM micrograph of MWNT after nitric acid treatment at (a) low and (b) high magnification.

acid [66]: thus the platinum particle size does not significantly change (2–3 nm) with the preparation method. MWNT supported, copper doped, iron catalysts have been prepared using incipient wetness or deposition/precipitation using urea and K_2CO_3 techniques; the sample obtained with the first two

methods led to the presence of nanoparticles of similar size (9–10 nm) whereas the last technique produced larger particles (34 nm) [67]. Reactions between H_2SO_4–HNO_3-treated MWNT and ethylene glycol solution of chloroplatinic acid were exploited to prepare 10% (w/w) Pt/MWNT catalyst; an homogeneous dispersion of spherical platinum nanoparticles was obtained with a narrow particle size distribution (2–4 nm) and an average size of 2.6 nm [68]. Clustered derived bimetallic nanoparticles (Ru-Sn and Ru-Pt) have been deposited from different organometallic precursors on oxidized MWNT; in the case of Ru-Pt/MWNT it has been found that the particles were homogeneously dispersed with a very small size of 1.8 ± 0.5 nm [69].

Nitric acid or preferentially nitric/sulfuric acid treatments have been proved to be effective for the creation of oxygen-containing surface groups on GNF-H and GNF-P: this treatment results in the formation of carboxylic and carboxylic anhydride groups. With GNF-P, in contrast with GNF-H, the macroscopic structure was severely affected by the mixed acid treatment [60]. Room temperature HNO_3 treatments have been realized on GNF in order to remove catalytic particles remaining from the production step, and it has to be noted that no information concerning the possible creation of functional groups responsible of anchoring is given [36,70,71]. Baker has deposited nickel nanoparticles by standard incipient wetness technique on GNF-P ($120\,m^2\,g^{-1}$), GNF-R ($85\,m^2\,g^{-1}$) and spiral-like GNF ($45\,m^2\,g^{-1}$) treated at room temperature for 7 days in diluted nitric acid. It is interesting to note that the measured sizes are equivalent to those reported for untreated supports [50,51], for example 8.1 nm for GNF-R, and that the obtained metallic particle sizes are not directly dependent on the surface area. Ruthenium-barium bimetallic catalysts supported on GNF ($140\,m^2\,g^{-1}$) treated in aqueous HNO_3 solutions were prepared from $RuCl_3{\cdot}xH_2O$ and barium nitrate, and the obtained particles were measured at 4–7 nm and located primarily on the outer surface. The same type of reaction was also used to prepare highly dispersed Ru/GNF with a narrow size distribution (2–4 nm) [71]. GNF-H with a $50\,m^2\,g^{-1}$ surface area have been treated for 2 h in HNO_3 at 80 °C and were used to support a 5% (w/w) palladium catalyst by incipient wetness impregnation from a palladium nitrate aqueous solution. The obtained spheroidal palladium nanoparticles display a narrow size distribution (1–11 nm) centered at around 5 nm. The authors have attributed this homogeneous dispersion to a relatively strong metal–support interaction between the metal salt precursor and the graphite edges of the nanofibers [72,73]. Curiously, the formation of carbon nodules on GNF after the reduction step (hydrogen, 350 °C) was also reported. Ion-exchange method from $[Pd(NH_3)_4][NO_3]_2$ is reported by Mojet et al. to prepare a 3% (w/w) catalyst on acid nitric treated GNF-R; after reduction, analyses pointed to the presence of small palladium particles of ca. 1.5 nm [74]. An EXAFS analysis of the freshly prepared catalyst, i.e. before the reduction step, showed a palladium tetraammine complex in interaction with the fiber surface. A stabilization of the cationic palladium species by the carboxylic acid groups, through OH bridges and charge balance, and by the π-electron system of the support is proposed. After the reduction step, significant palladium carbon interactions are observed. Very small rhodium metallic particles (1.1–2.1 nm) were obtained on HNO_3–H_2SO_4 surface oxidized GNF-H by impregnation or ion-exchange methods from $RhCl_3{\cdot}3H_2O$ solutions [75]. The important role of surface oxidation is emphasized by the fact that no rhodium particles were deposited on untreated GNF-H pointing to the lack of interaction between the metal precursor and the graphitic surface.

3.2.2. Other oxidative treatments

Besides the classical nitric acid treatments other oxidative agents have been used to prepare functionalised CNT. Rao and co-workers have compared the effect of concentrated nitric acid, concentrated sulfuric acid, aqua regia, HF–BF_3, aqueous OsO_4 and $KMnO_4$ (acid/alkali) solutions on MWNT's structures [76]. All these oxidants effectively opened the nano-tubes but, the essential structural features were still present at the end of the treatment. The advantage of HF–BF_3 super acid and OsO_4 is that the reaction can be conducted at room temperature. In the case of osmylation, theoretical calculations have predicted the formation of osmate ester adducts via complexation on the CNT's walls through a base-catalyzed cycloaddition reaction [77]. The concentration of the surface acid groups, after 24 h of treatment under reflux, has been measured to be 2.5×10^{20} for HNO_3, 6.7×10^{20} for H_2SO_4, 7.6×10^{20} for aqua regia and $(8–10) \times 10^{20}$ sites per gram of MWNT for a $KMnO_4$ (acid/alkali)

solution. The authors also report attempts to fill these open ended nanotubes with different metals such as silver, gold, platinum and palladium by simple impregnation procedures. A recent report on the use of potassium permanganate solutions as functionalizing agent for MWNT stresses the improvements that can be achieved by adding a phase transfer agent during the reaction [78]. XPS results show that the yield of functionalization is increased from 35 to 65%. Liu and coworkers have oxidized CNT surface by treatments with different agents like HNO_3, HNO_3–H_2SO_4 and $K_2Cr_2O_7$–H_2SO_4 [79]. XPS analyses have demonstrated that the HNO_3–H_2SO_4 treatment can lead to the formation of sulfur containing species on the surface; additionally, because of the excessive oxidative strength of this solution, it has been found that most of the raw material is destroyed (40% after 6 h and 100% after 24 h) resulting in low oxidation yields. The yields of functionalised MWNT were 93 and 91% for HNO_3 and $K_2Cr_2O_7$–H_2SO_4, respectively. After a sensitization process with $SnCl_2{\cdot}2H_2O$, platinum nanoparticles (1–5 nm) were successfully deposited on the modified MWNT.

3.2.3. *Grafting of organometallic complexes on CNT and GNF and other methods*

The immobilization of organometallic complexes on CNT or GNF normally requires a pre-emptive surface oxidation or modification step before any complexation reaction. The coordination modes of $[IrCl(CO)(PPh_3)_2]$ on(to) untreated and $KMnO_4$ modified SWNT were studied by Wong and Banerjee [80]. On pristine nanotubes pentacoordination is proposed with η^2-coordination by one C–C double bond (see Fig. 5a); while on treated SWNT the hexacoordinated Ir(III) structures prevail resulting from the oxidative addition reaction (see Fig. 5b). A recent DFT study has shown that η^2-bonding of metal fragments to nanotubes is weak, making questionable the stability of η^2-complexes of CNT [21]. A similar procedure was also used to graft the Wilkinson complex $[RhCl(PPh_3)_3]$ on SWNT and here again the formation of an hexacoordinated rhodium species is proposed from NMR data [81].

Preparation of a rhodium complex grafted on nitric acid-treated MWNT by impregnation from a $[HRh(CO)(PPh_3)_3]$ benzene solution has been reported by Zhang et al., although it was poorly characterized [82]. The reaction between amino ($–NH_2$) groups functionalised MWNT and a ruthenium complex, produced by reaction of [ruthenium(4,4′-dicarboxy-2,2′-bipyridine)(2,2′-bipyridyl)$_2$]$(PF_6)_2$ and thionyl chloride, has been reported in order to obtain a grafted compound (see Fig. 6) [83]. A different approach was used by Koningsberger and co-workers to achieve the immobilization of a rhodium complex on

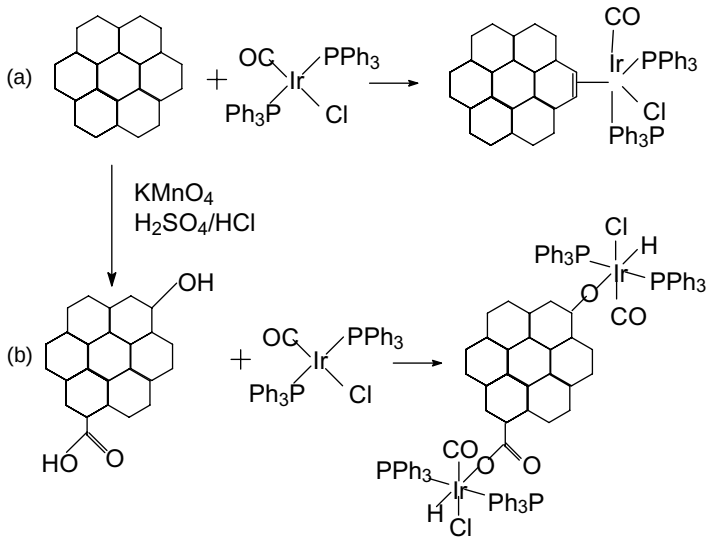

Fig. 5. Coordination modes of $[IrCl(CO)(PPh_3)_2]$ (a) on untreated and (b) $KMnO_4$ modified SWNT.

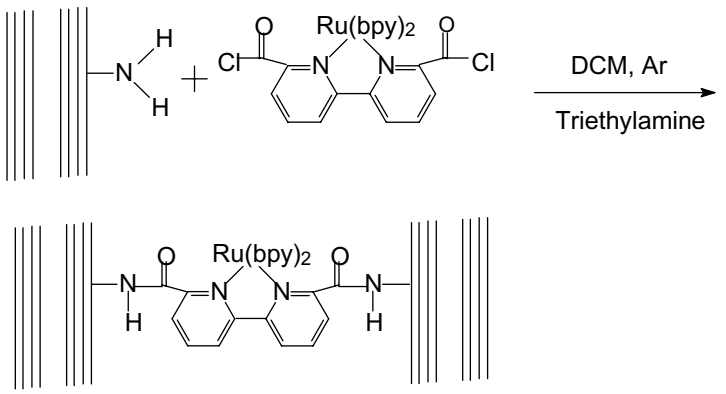

Fig. 6. Surface reaction between the amino groups of modified MWNT and a ruthenium complex.

HNO_3–H_2SO_4 treated GHF-H [84]. The multi-step synthesis consists in: (i) conversion of the surface carboxylic acid groups into acid chloride groups by reaction with thionyl chloride, (ii) attachment of anthranilic acid to the GNF-H surface through reaction with the acid chloride groups and (iii) complexation of the anthranilic acid ligand to rhodium by reaction with rhodium chloride (see Fig. 7). An hexacoordinated rhodium complex is proposed, anthranilic acid coordinates to rhodium trough the nitrogen atom and the carboxyl group, the coordination sphere being completed by three water molecules and a chloride ion. Further reduction of rhodium with sodium borohydride results in the formation of rhodium nanoparticles with an estimated diameter of 1.5–2 nm on the GNF-H. The preparation of a rhodium catalyst supported on MWNT by a surface mediated organometallic reaction (see Fig. 8) was recently reported by Giordano et al. [62]. Nitric acid-treated MWNT were reacted with sodium carbonate in order to produce sodium carboxylate groups, the surface reaction between $[RhCl(CO)_2]_2$ and these carboxylate groups leading to NaCl elimination and to the formation of ill-defined anchored carbonyl species that upon hydrogen reduction generate highly dispersed rhodium nanoparticles (1.5–2.5 nm). Worth to be noted is that when using this grafting method good dispersions and small particle sizes (3 ± 2 nm) can be achieved also with high metal loading (up to 10% (w/w)) (see Fig. 9).

A sophisticated method was recently reported for the deposition of gold nanoparticles (10 nm) on nitrogen doped carbon nanotubes (CN_x) [85]. After a nitric/sulfuric acid treatment, a cationic polyelectrolyte, poly(diallyldimethylammonium)chloride, was

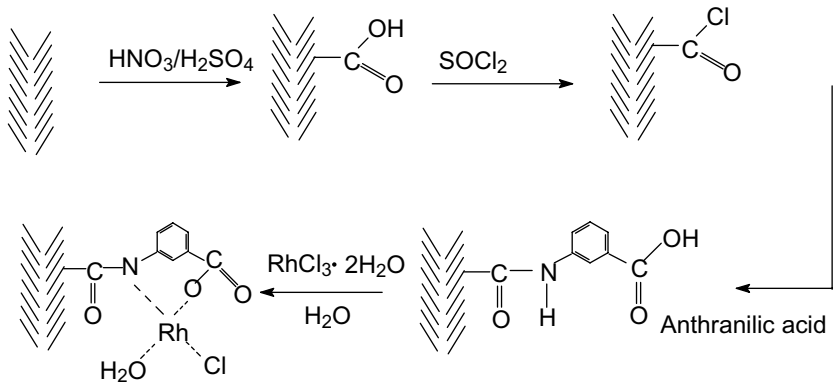

Fig. 7. Multi-step synthesis for the immobilization of a rhodium complex on GNF-H.

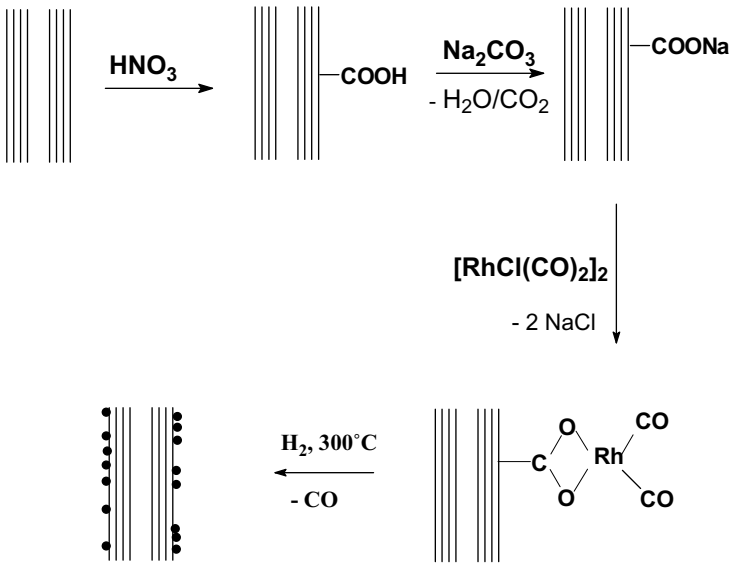

Fig. 8. Surface mediated organometallic reaction between a rhodium complex and modified MWNT.

adsorbed on the surface of the nanotubes by electrostatic interactions. A further reaction between the modified surface and negatively charged gold nanoparticles from a gold colloid suspension led to the formation of the final material by electrostatic interactions. Due to ionic character of the bonding, a weak metal–support interaction can be predicted. The surface of MWNT has been modified by adsorption of polyethyleneimine which presents positively charged amino groups (NH_2^+); such a support was used to deposit TiO_2 with a mean particle size ranging between 2 and 10 nm by controlled hydrolysis and condensation of titanium bis-ammonium lactato dihydroxide [86].

To conclude, it appears well established that different efficient synthetic routes are at the disposal of chemists to prepare supported metal catalysts on CNT

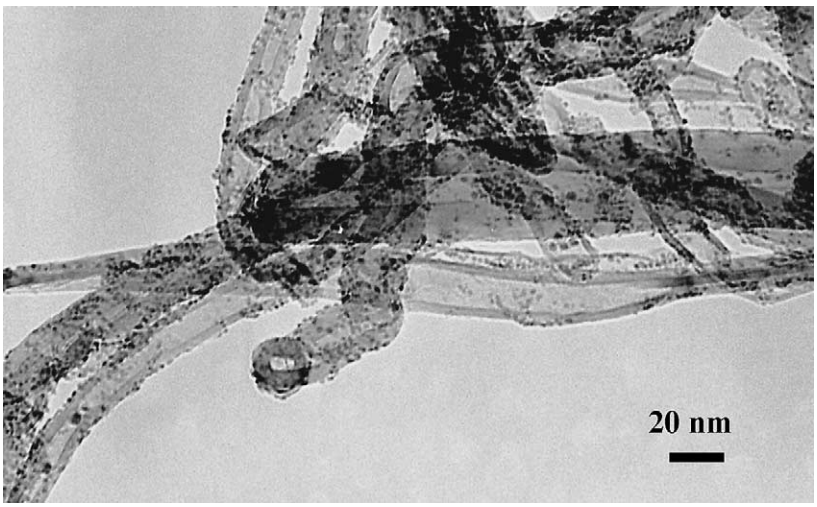

Fig. 9. TEM micrograph of a 10% (w/w) Rh/MWNT.

or GNF. Although it seems clear that oxidative surface treatments of the supports improve the dispersion of the metallic phase, it is important to consider that a precise comparison between the various materials is a very difficult task since the preparation processes may significantly affect some of their characteristics such as purity, porosity and surface area.

4. Catalytic performances of CNT- and GNF-based catalysts

Considering the advantageous properties of CNT and GNF as supports discussed previously several studies have been carried on different catalytic reactions. Particularly, a lot of attention has been dedicated to liquid-phase reactions with MWNT and GNF supported catalysts; indeed, their high external surface and their mesoporosity should allow significant decreases on mass-transfer limitations when compared to activated carbon. It is also relevant that very few studies dealing with SWNT supported catalytic systems have been reported, due either to their microporosity or to the fact that it is still very difficult to obtain large enough quantities of pure material to conduct catalytic studies. In this section, we will present the obtained results according to the reaction type and, when possible, we will attempt to rationalize these results by comparison with other carbonaceous supports. Representative catalytic studies using CNT and GNF based catalysts are presented in Table 3.

4.1. Hydrogenation reactions

The most studied reaction with SWNT, MWNT and GNF, both in liquid and gas phase, is hydrogenation and two types of reactions have to be taken into account: alkenes hydrogenation or α,β-unsaturated aldehydes selective hydrogenation.

The research team of Baker has conducted several studies on light alkenes such as ethylene, but-1-ene and buta-1,3-diene hydrogenation on nickel catalysts supported on different types of GNF (GNF-R, GNF-P or spiral-like GNF), γ-alumina and activated carbon [36,50,70]. The authors state that the nickel crystallite's activity and selectivity can be altered greatly by the interactions with the support; indeed, it was found that the catalyst supported on GNF allows higher conversion, compared to those obtained with γ-alumina and activated carbon supported systems, even if the metallic particle size is larger (6.4–8.1 nm for GNF, 5.5 nm for activated carbon and 1.4 for alumina). These results point to the fact that catalytic hydrogenation might be a structure sensitive reaction. HTEM studies have been conducted in order to get insights onto the metallic particles morphology: on GNF supports the deposited crystallites were found to adopt very thin, hexagonal morphologies, and since

Table 3
Selected examples of catalytic results

Catalyst	Particle size (nm)	Reaction	Comments	Reference
Ni/GNF	6–8	Butene hydrogenation	Higher conversion compared to Ni/Al_2O_3 and Ni/C* with lower particle size	[36,50]
Rh/MWNT	1.5–2.5	Cinnamaldehyde hydrogenation	Catalytic activity three times higher than a corresponding Rh/C* catalyst	[62]
Rh/MWNT	11	NO decomposition	Higher conversion than with a Rh/Al_2O_3	[95]
Rh/GNF	15	Ethylene hydroformylation	Higher selectivity towards aldehydes and comparable activity in respect to Rh/SiO_2	[53]
Co/MWNT	5	Cyclohexanol dehydrogenation	Activity and selectivity towards cyclohexanone slightly higher then on Co/C*	[91]
Pt/GNF	12	Skeletal *n*-hexane reaction	Higher selectivity towards isomers in respect to a Pt/SiO_2 catalyst (EUROPT-1)	[54]
Pt/GNF	<10	Methanol oxidation	400% higher conversion than a Pt/Vulcan carbon electrode	[18]
Ni/GNF	30–70	Methane decomposition	A 15% (w/w) Ni/GNF has a comparable activity with a 90% (w/w) Ni/Al_2O_3	[101]

the electron density was homogeneous across a given particle it might be concluded that they were relatively flat. These growth features are generally believed to generate in situations where a strong metal–support interaction is present that induces a spreading of the metal on the support surface. In contrast, a more globular particle geometry was prevalent when nickel was supported on γ-alumina, consistent with the existence of a somewhat weaker metal–support interaction. Additionally, the authors propose that the extremely small particle size obtained on alumina could be responsible for a strong adsorption of but-1-ene and buta-1,3-diene resulting in a low catalytic activity. Differences on the activity were also found between the catalytic systems prepared on the different type of nanofibers. For example, for the hydrogenation of buta-1,3-diene ($C_4H_6/H_2 = 1/2$) on a 5% (w/w) catalyst, high conversions were obtained on GNF-P and spiral-like GNF whereas the GNF-R supported system gave dramatically lower conversions. This difference of behavior disappears in the case of ethylene hydrogenation. Whereas the authors admit that further studies are compulsory to clearly explain the unexpected performances of the GNF supported nickel systems, they propose that a high concentration of adsorption sites for metallic particles is present on the fibers and that two different types can be distinguished: namely zigzag and armchair faces (see Fig. 10). Since the ratio between zigzag and armchair will vary with the type of GNF structure, dramatic changes in catalytic activity and selectivity may be explained in terms of nucleation and growth of nickel particles on the different structures of the supports. A more specific study has been realized on GNF-P by selective chemical blocking of the two types of faces with boron oxide or phosphorous compounds from ammonium pentaborate and methyl-phosphonic acid, respectively [36]. It has been found that the incorporation of boron oxide, which results in blocking the zigzag sites, rendered the catalytic system virtually inactive towards hydrogenation of the olefins, meaning that it is on this type of face that nickel is more active. This explanation was also confirmed by TEM analyses where the previously described geometry (thin hexagonal particles) was observed on untreated and phosphorous treated samples but was not found on the boron blocked GNF where nickel is assumed to have a globular shape.

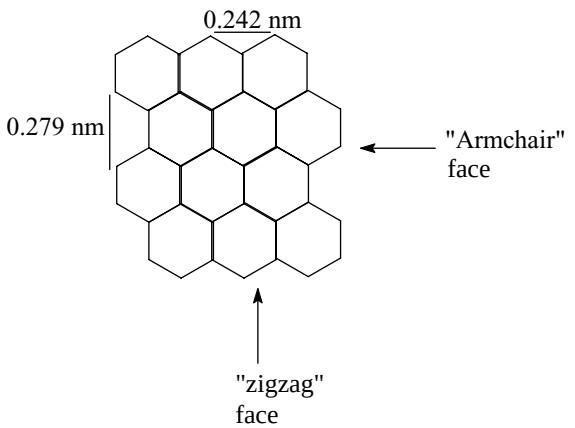

Fig. 10. Different adsorption sites on GNF.

Oxidized GNF-H supported rhodium nanoparticles (1.1–2.2 nm) were used as catalytic system to study the hydrogenation of cyclohexene [75]. These catalysts turned out to be extremely active even at low hydrogen pressure with low metal loadings (1% (w/w)) and low cyclohexene concentrations (1% v/v). The authors propose that the activity is almost independent of the nanoparticles sizes and that other factors like the possible clustering of the support in the liquid phase and the influence of oxygen-containing species present on the surfaces of the support are responsible for the final results. A similar Rh/GNF-H catalyst, prepared under mild conditions, displayed comparable activity for the same reaction [84]. Unfortunately, no comparison with similar activated carbon supported catalyst is provided in both reports.

The hydrogenation of α,β-unsaturated molecules on GNF or CNT supported catalysts was the object of several studies. Gas phase hydrogenation of crotonaldehyde to crotyl alcohol was conducted between 75 and 150 °C on a 5% (w/w) Ni catalyst supported on GNF-P, GNF-R and γ-alumina [51]. Even if the mean particle size differs largely depending on the support, from a narrow distribution centered on 1.4 nm for γ-alumina to broad distribution centered on 7 nm for GNF, higher selectivity and activity were obtained on the GNF supported catalysts. This difference is attributed to the fact that, for GNF, nickel particles are located on the edge sites of the support: thus it might be expected that different crystallographic faces of the metal will be exposed to the reactants. Additionally,

the possibility that electronic perturbations induced by the support could lead to different activities has been proposed. The homogeneous deposition precipitation technique was used to deposit highly dispersed ruthenium nanoparticles (<3 nm) on nitric acid oxidized GNF-H and the activity of this catalyst in cinnamaldehyde hydrogenation was investigated [87]. After a hydrogen reduction at 200 °C, the samples were heated under nitrogen between 300 and 700 °C for 2 h, in order to eliminate the oxygen-containing groups by CO and CO_2 evolution. It was found that the catalysts treated at 400 °C were 22 times more active than the untreated system; also a decrease of the selectivity towards cinnamyl alcohol (from 48 to 8%) was evidenced pointing out the crucial role of the surface oxygen-containing functionalities. As ruthenium is well known to enhance the selective hydrogenation of the C=O bond, the exact mechanism of this phenomenon is not trivial. The authors have stressed the importance of the catalyst's post-treatments on their activity and selectivity. A palladium supported catalyst on GNF-H ($50\,m^2\,g^{-1}$) or activated carbon ($1000\,m^2\,g^{-1}$) was used in the liquid-phase hydrogenation of cinnamaldehyde to hydrocinnamaldehyde [72,73,88,89]. The higher performances of the GNF supported catalyst in terms of activity and particularly selectivity (90% compared to 40% for activated carbon) are explained by the absence of mass-transfer limitations compared to the microporous activated carbon, and, also in this case, a peculiar graphitic carbon–palladium interaction in addition to some residual acidity on the activated carbon surface might have favored some CO bond hydrogenation. When using a 1% (w/w) Rh/MWNT for the same reaction a selectivity of 100% was obtained and the catalytic activity of the MWNT ($180\,m^2\,g^{-1}$) based catalyst was three times higher than that of a 1% (w/w) Rh/C* where the support has a surface area of $700\,m^2\,g^{-1}$ [62]. The importance of the pre-treatment of the support was also emphasized by comparing the activity of rhodium catalysts prepared on untreated MWNT (particle size up to 100 nm) where no activity was found, nitric acid-treated MWNT (particle size 2.5–5 nm) which had an activity of $27\,g_{substrate}\,g_{Rh}^{-1}\,h^{-1}$ and MWNT functionalised with –COONa groups (particle size 1.5–2.5 nm) that was the most active with a value of $78\,g_{substrate}\,g_{Rh}^{-1}\,h^{-1}$. In this case, the importance of the metal dispersion on the graphitic support has been stressed. Unpurified nanotubes coming from arc discharge evaporation of graphite ($27\,m^2\,g^{-1}$) were used to support ruthenium to conduct the same reaction [42]. This catalytic system was compared to Ru/alumina and Ru/C* catalysts presenting similar metallic particle sizes (3.5 nm): the selectivity for cinnamyl alcohol were 92, 20–30 and 30–40%, respectively. SWNT grown by arc method, containing platinum and cobalt coming from the production step, were used to study the selective hydrogenation of cinnamaldehyde to cinnamyl alcohol [90]. A catalytic system containing 7% (w/w) cobalt and 5.4% (w/w) platinum and presenting a mean particle size(s) of 8 nm allows to reach 80–85% molar selectivity towards the desired product. Furthermore the initial cinnamyl alcohol selectivity, close to 100%, but not reported for PtCo/C* catalytic system, might indicate the presence of some peculiar SWNT–metal(s) interactions. Finally, a platinum supported catalyst on purified SWNT was shown to be active and selective in the hydrogenation of prenal (3-methyl-2-buthenal) to prenol (3-methyl-2-buthenol) [61].

4.2. Other reactions

Besides hydrogenation, other "classical" chemical reactions using CNT or GNF supported catalysts have been investigated.

Selective dehydrogenation of cyclohexanol to cyclohexanone was studied with a cobalt CNT based catalytic system [64,91]. The effect of the oxidizing pre-treatment of the support surface on the catalytic performances of the system has been evidenced; the smaller particle size obtained on the nitric acid-treated MWNT, 5 nm instead of 100 nm on untreated support, allows an almost 20% higher conversion. A comparison between a 15% (w/w) Co/MWNT and the corresponding Co/C* has been made: a slightly higher selectivity to cyclohexanone was found for the former catalytic system, as well as a different by-products distribution. Rhodium supported catalysts on GNF-H, GNF-P or GNF-R were used to study the hydroformylation of ethylene and to permit a comparison with a Rh/SiO_2 system [53]. As in the case of hydrogenation [36,50,70], even if silica has an higher specific surface area and the nanoparticles are smaller on this support, it was found that the GNF supported catalysts exhibit an higher selectivity and a comparable catalytic

activity. It is believed that the hexagonal shape of the rhodium crystallites evidenced on GNF is responsible for the better results obtained. Additionally, it can be noted that, among the GNF, it is the GNF-R support (lowest surface area) that displays the highest selectivity. No clear explanation concerning this behavior is given and this results could not be predicted by a correlation between the support surface area/particle size and the catalytic activity. Rhodium nanoparticles deposited on surface modified MWNT were used to perform the hydroformylation of hex-1-ene [62]. It is reported that this highly dispersed catalyst (1% (w/w), 1.5–2.5 nm) is more active than a Rh/C* catalyst prepared by a similar procedure. The authors propose that the mesoporous nature of the MWNT, compared to the microporous texture of activated carbon, contributes to better performances by increasing the transfer processes. The complex $[HRh(CO)(PPh_3)_3]$ has been grafted on MWNT and GNF-H and the catalytic activity in propylene hydroformylation was compared with the one of a similar system prepared on activated carbon, carbon molecular sieves and silica [82]. Higher conversion and regioselectivity towards *n*-butylaldehyde are reported for the MWNT and GNF supported systems. The authors propose that the nanotube channel's size fits to accommodate the rhodium complex and to prevent extensive capillary condensation of *n*-butylaldehyde compared to the other supports. No details are given concerning the possible leaching of complex from the support to the solution. Interestingly, a positive effect of MWNT on homogeneous oxidation of cyclohexene catalyzed by a ruthenium complex has been recently reported [92]. The authors have noted that the 20–25 nm external diameter nanotubes have no catalytic activity for this reaction but their addition to an active homogeneous ruthenium complex can enhance the conversion of cyclohexene and the selectivity to 2-cyclohexen-1-ol, and improve the recycling of the ruthenium complex. The possibility of an in situ grafting of the metallic complex on the oxidized MWNT has to be taken into account to explain these results. The activity of MWNT supported copper doped iron catalysts has been studied in the Fischer–Tropsch reaction [67]. The deposition of the active phase was conducted by three different techniques leading to different particle sizes; it was found that the catalytic activity depends on this characteristic, whereas the selectivity was size independent. Ruthenium based catalysts supported on GNF [71] or MWNT [93] were used for ammonia synthesis and compared to other carbon based supports (graphite, fullerenes and activated carbon). Potassium promoted ruthenium catalysts supported on MWNT were found to be much more active than their counterparts deposited on graphite (4 or 5 times higher) or fullerenes (10 times greater). This difference has been attributed to the higher surface area of nanotubes that allows a better dispersion of the metallic phase and to the electronic properties of this support that could enhance the electron transfer from potassium to ruthenium [93]. Barium was also used as promoter for a Ru/GNF catalytic system [71], the activity and stability of this system for ammonia synthesis was higher compared to the one of a similar catalyst supported on activated carbon. A good dispersion of the active phase, with a narrow size distribution 2–4 nm, together with the high purity of the support are believed to be responsible for these remarkable results. Indeed, it is suggested that the surface impurities of activated carbon such as sulfur, nitrogen, oxygen or chloride can reduce the catalytic activity by consuming part of the promoter. The catalytic decomposition of hydrazine was studied on iridium deposited on carbon nanofibers supported on graphite felt [57]. The better performances of the carbon composite supported catalyst, compared to a commercial high surface area alumina based catalyst presenting similar metallic particle size, were attributed to both the absence of any detrimental microporosity on the carbon composite support and the presence of peculiar metal–support interactions. Another interesting characteristic of this system is its high stability due to the good mechanical properties of the carbon support compared to alumina. Finally, the sintering of iridium particles was much less pronounced in the case of the graphite felt support. Skeletal *n*-hexane reaction was investigated by using a 5% (w/w) platinum supported catalyst on GNF-P, and the results were then compared to those obtained with a EUROPT-1 catalyst (6% (w/w) Pt/SiO_2) [54]. The main difference resides in the selectivity, since the GNF supported catalyst favors the formation of isomers at lower temperature and higher hydrogen pressures. This result, as well as the absence of multiple fragmentation and enhanced propane formation points to an higher H surface concentration in the case of GNF, that may be correlated

to the hydrogen storage capacity reported for such a material [94]. The reduction of NO by hydrogen was performed by using either MWNT (194 $m^2 g^{-1}$) or 1% (w/w) Rh/MWNT (140 $m^2 g^{-1}$) [95]. Nanotubes alone displayed only a moderate activity (8% conversion at 300 °C) for NO decomposition and Rh/MWNT allowed a better conversion (21%), higher than a 1% (w/w) Rh/Al_2O_3 (12%). XPS analyses indicated that MWNT are more suitable for maintaining rhodium in its metallic state and therefore to favor NO decomposition. Carbon granules consisting in agglomerates of carbon filaments (70–140 $m^2 g^{-1}$) produced on nickel catalyst [96] have been used for the direct selective hydrogenation of hydrogen sulfide [97]. The activity of this catalytic system can decrease due to sulfur poisoning of the most active adsorption sites.

4.3. Fuel cell electrocatalyst

CNT and GNF can also be used efficiently as metal–supports in fuel cell electrodes in order to replace the classically used carbon blacks. Two types of metals, platinum and ruthenium, or a combination of them, have been tested in both direct methanol oxidation and oxygen reduction. Platinum (5% (w/w)) was supported on GNF-P, GNF-R and GNF-H with the aim to be used as electrodes in fuel cells [18]. The authors exploited a direct methanol oxidation at 40 °C as probe reaction and compared the results obtained on the GNF supported electrocatalysts with similar electrodes based on a commercial carbon black (Vulcan carbon with a 267 $m^2 g^{-1}$ surface area). The results evidence that the GNF-P and GNF-R based electrodes display higher activities than the ones on Vulcan carbon (400% better results) and GNF-H, that showed almost no electrocatalytic activity. Even if the exact reasons for such results are not yet fully cleared, several explanations have been proposed by the authors. A first parameter that has got to be taken into account is the geometry of the metallic particles on the support: the particles found on GNF presented a thin, highly crystalline faceted structure that can be associated to a strong metal–support interaction, whereas on Vulcan carbon the metal was found to adopt a more dense globular morphology. The different behavior of the GNF supports is also considered: P-type and R-type fibers expose mainly edge-sites to the reactants favoring the oxidation; the H-type fibers on the contrary has an hydrophilic nature that might explain the very low activity. Finally, a consideration on the self-poisoning of the catalyst has been investigated and has shown a direct correlation with the electrocatalytic activity: carbon black, always containing impurities, is more sensitive to poisoning when compared to the sulphur-free GNF. The same reaction was also conducted with a 10% (w/w) Pt/MWNT cathode and the results were compared with the ones obtained on an identical electrode where platinum was supported on a commercial Vulcan carbon [68]. The results show that CNT support allows to obtain higher power density in comparison to carbon black based electrode (approximately six times higher); the authors have also conducted tests using an electrode made exclusively of MWNT and have demonstrated that it does not show any electrocatalytic activity. The possible explanations for this behavior are related to the unique properties of MWNT that can increase the conductivity of the electrode and the high purity of the support when compared to carbon black. Four platinum-ruthenium carbon composites were prepared as anode catalysts by using a molecular hetero-bimetallic precursor as a metal source [56]. Different carbonaceous materials like SWNT, MWNT, GNF-P and GNF-H were tested as supports and compared to an unsupported platinum-ruthenium colloid. The samples having some degree of ruthenium metal face segregation have given the highest electrocatalytic performances and the best results were obtained when using narrow tubular GNF-H support (64% greater than the unsupported colloid). Relatively small particle sizes were measured on all supports even at very high metal loadings (40–60% (w/w)). Surprisingly, low surface area are reported for SWNT (109 $m^2 g^{-1}$) and especially MWNT (8 $m^2 g^{-1}$) that could be related to a poor quality material. No explanation for these different behaviors have been proposed. A template method was used to prepare: (i) 200 nm diameter MWNT and (ii) platinum (7 nm) or platinum-ruthenium (1.6 nm) filled MWNT fuel cell anode [98]. The current density of methanol oxidation for a platinum supported on MWNT membrane electrode was found to be 20 times higher than that of a bulk platinum electrode. This material can also be used to electrocatalyze oxygen reduction. A template method was also used to prepare tubular carbon structures–alumina composites

which were filled with platinum (1.2 nm particles), platinum-ruthenium (1.6 nm) or platinum–tungsten (10 nm) oxide in order to be used as electrodes in methanol oxidation [99,100]. The authors have found that the electrochemical activity follows the order: Pt-WO_3/CNT > Pt-Ru/CNT > Pt/CNT. They have also compared the activities and stabilities with those of electrodes prepared from commercial carbons such as Vulcan or E-TEK carbon [100]. In this case, the order for activity and stability is Pt-WO_3/CNT > Pt-Ru/E-TEK-Vulcan > Pt/CNT > Pt/E-TEK-Vulcan > bulkplatinum. The higher electrochemichal response of CNT based materials has been correlated to the higher available electroactive surface area. Platinum supported on activated MWNT was used as a cathode electrocatalyst for oxygen reduction in a fuel cell [79]. In the absence of any metal, no activity was measured and the authors propose that the functionalization of the nanotubes is important to obtain an efficient Pt/MWNT catalyst. XPS analysis showed that platinum was present in both Pt(0) (67%) and Pt(IV) (33%) states.

4.4. Catalytic decomposition of hydrocarbons

A relevant problem connected to carbon nanotubes production on supported catalysts on an industrial scale is the purification step required to remove the support and possibly the catalytic phase from the obtained material. To avoid this costly operation the use of CNT or GNF supported catalysts for CNT or GNF production has been investigated [52,55,101–104].

Iron nanoparticles (12.4 nm, 10% (w/w)) supported on GNF (184 $m^2\,g^{-1}$) were compared to a similar system supported on γ-alumina (particles of 5.3 nm and BET surface area 91 $m^2\,g^{-1}$) for the conversion of hydrocarbons to solid carbon at 600 °C from a $CO/C_2H_4/H_2$ mixture [55]. Dramatic differences have been evidenced for these two catalytic systems. While high conversions towards solid carbon (80%) were measured for both systems, a severe deactivation occurred on the alumina supported catalyst after 20 min on stream. The catalytic activity of the GNF-based system remained constant even after 150 min of reaction. Furthermore, TEM observations of the solid carbon have evidenced that the deposit consists exclusively of tiny carbon nanofibers; however the Fe/GNF catalyst allows an higher selectivity towards the CNT formation. Nickel was deposited onto carbon nanofibers by wet impregnation from nitrate and chloride salts and was then used to study methane decomposition in order to obtain solid carbon [101]. The authors have found that the catalytic activity of the chloride based catalyst (15% (w/w) and BET surface of 100–115 $m^2\,g^{-1}$) was similar to the one reported for a Ni/Al_2O_3 system (90% (w/w) and BET surface of 105 $m^2\,g^{-1}$). MWNT pellets of 100–200 $m^2\,g^{-1}$ prepared by hot pressing (10 mm × 10 mm × 1 mm) have been used as supports to deposit nickel from a nitrate aqueous solution [102]. This catalytic system was found to be active in propylene decomposition to lead to the formation of 50–300 nm outer diameter GNF. The production of GNF with a controlled diameter of about 50 nm and a specific surface area ranging between 100 and 150 $m^2\,g^{-1}$ has been achieved from ethane decomposition on a nickel supported catalyst on low surface area (10 $m^2\,g^{-1}$) and large diameter (100–150 nm) MWNT [103]. Acetylene decomposition was investigated using several commercial SWNT samples of different purities as catalysts or catalysts supports [104]. On the raw material containing from 15 to 70% of SWNT and remaining metal impurities, very low selectivity towards CNT or GNF has been observed. When iron, cobalt or nickel were added to the support by impregnation, it was found that acetylene decomposition led to the quite selective formation of MWNT on the 70% purity support, whereas the less pure SWNT-based system gave different carbon structures. Interestingly, in several samples the authors have noticed the disappearance of the SWNT support and proposed that they were “absorbed” into GNF or MWNT. It can also be advanced that the support acts as a template for carbon deposition. Several carbon supports were used to study methane decomposition on 20% (w/w) nickel catalyst [52]. The catalytic activity expressed as $g_C\,g_{Ni}^{-1}$ followed the order: Ni/graphite carbon fibers ($S_{BET} < 10\,m^2\,g^{-1}$) 60 $g_C g_{Ni}^{-1}$, Ni/GNF ($S_{BET} = 77\,m^2\,g^{-1}$) 46 $g_C\,g_{Ni}^{-1}$, Ni/vapor grown carbon fibers ($S_{BET} < 10\,m^2\,g^{-1}$) 9 $g_C\,g_{Ni}^{-1}$, Ni/graphite powder ($S_{BET} = 1.7\,m^2\,g^{-1}$) 6 $g_C\,g_{Ni}^{-1}$, Ni/C* ($S_{BET} = 890\,m^2\,g^{-1}$) 0.2 $g_C\,g_{Ni}^{-1}$. The low activity measured for activated carbon supported catalyst can be attributed to diffusion limitations in the micropores. It should be noted that the solid form of carbon that was obtained on the fiber based systems is mainly constituted of GNF. MWNT grown over

iron-molybdenum catalysts, containing 10 % (w/w) of remaining metal (atomic ratio Fe/Mo = 2/3), were used to catalytically decompose methane [105]. It was found that this system is active for the preparation of MWNT with similar geometrical features than the pristine material. As-prepared and acid-treated (hydrofluoric and sulphuric) MWNT were used as supports for nickel to form a catalytic system used in propylene decomposition to form CNT [106]. The effect of the acid treatment seems to improve the catalytic activity and selectivity as well as the quality of the products. Indeed, the acid-treated supported catalyst has an higher surface area ($S_{BET} = 189\,m^2\,g^{-1}$) with respect to the one of the as-prepared MWNT based one ($S_{BET} = 133\,m^2\,g^{-1}$) with smaller nickel nanoparticles (8.5 nm compared to 10.4 nm). The yields were 50% higher and the geometrical features of the CNT more regular. The authors propose that this different behavior is correlated to the presence of functional groups on the treated supports that reduce the hydrophobic nature of MWNT and make the surface more accessible to the metallic precursors solutions resulting in a better dispersion.

4.5. CNT or GNF as heterogeneous catalysts

Besides their use as supports, CNT or GNF have been used as direct catalysts in methane decomposition [107] or oxidative dehydrogenation of ethylbenzene to styrene [108]. MWNT samples (containing 10–40% of nanotubes with 7–12 nm external diameter) were used to obtain CO and CO_2 free hydrogen from methane decomposition. A comparison with 30 different samples of elemental carbon including a variety of C*, carbon blacks or fullerenes, has been reported [107]; it was found that disordered forms of carbon are generally more active than the ordered ones and that the activity is structure and surface area dependant. Relatively low conversions were obtained on the low purity MWNT samples. In the dehydrogenation reaction [108] GNF ($47\,m^2\,g^{-1}$) catalysts were compared to graphite ($69\,m^2\,g^{-1}$) and soot ($19\,m^2\,g^{-1}$). It is reported that GNF display a high stability towards oxidation, and higher activity and selectivity when compared to the two other tested materials. However, no comparison are given with activated carbons, which are commonly considered as efficient catalysts for this specific type of reaction.

Finally, it has been reported that, although not directly implicated, MWNT can improve the catalytic activity of a $Cu/ZnO/Al_2O_3$ system for methanol synthesis [109]. Indeed, the addition of 10–15% (w/w) of MWNT to the catalyst allows to reach higher CO conversions and methanol productivity. A possible explanation could be that the highly conductive MWNT might promote hydrogen spillover from the Cu sites to the Cu/Zn interphasial active sites, and thus be favorable for increasing the CO hydrogenation reaction rates.

5. Conclusions

Even if industrial production of nanotubes or nanofibers has not yet been achieved, the current synthesis processes for MWNT and GNF allow to foresee the attaint of this goal in a short lapse of time. Although the production processes are more and more controlled, it is still very difficult to have an homogeneity in all the characteristics (geometrical, purity, ...) of these materials, so that a precise comparison between different samples of different origins is hazardous. Concerning the preparation of supported catalysts, several methods have been successfully used, and, as in the case of activated carbon, the role of surface pre-treatments on the final metal dispersion has been clearly demonstrated. The catalytic studies conducted on CNT or GNF based systems have shown encouraging results in terms of activity and selectivity. In particular, high selectivity have been obtained on catalytic systems displaying larger particle size than those found on other supports such as activated carbon or alumina. From this literature survey, the main advantages of CNT or GNF supports compared to activated carbon are: (i) the high purity of the material can avoid self-poisoning, (ii) the mesoporous nature of these supports can be of interest for liquid-phase reactions, thus limiting the mass transfer, and (iii) specific metal–support interactions exist(s) that can directly affect the catalytic activity and the selectivity. Unfortunately, a lack of systematic comparison with activated carbon based catalytic systems has to be noted and should be considered in the future studies as it is a necessary step towards an extensive use of these new materials. Additionally, in many studies the comparisons reported were not carried out by using turn over

frequency for activity or at isoconversion in consecutive reactions which alters the meaning of selectivity patterns, in particular for hydrogenation reactions.

References

[1] F. Rodriguez-Reinoso, Carbon 36 (1998) 159.
[2] E. Auer, A. Freund, J. Pietsch, T. Takke, Appl. Catal. A 173 (1998) 259.
[3] R. Schlögl, in: G. Ertl, H. Knözinger, J. Weitkamp (Eds.), Preparation of Solid Catalysts, Wiley-VCH, Weinheim, 1999, p. 150.
[4] M. Hillert, N. Lange, Zeitschr. Kristall. 111 (1958) 24.
[5] P. Schützenberger, L. Schützenberger, C. R. Acad. Sci. Paris 111 (1890) 774.
[6] C. Pelabon, H. Pelabon, C. R. Acad. Sci. Paris 137 (1903) 706.
[7] S. Iijima, Nature 354 (1991) 56.
[8] S. Iijima, T. Ichihashi, Nature 363 (1993) 603.
[9] D.S. Bethune, C.H. Kiang, M.S. de Vries, G. Gorman, R. Savoy, J. Vasquez, R. Bayers, Nature 363 (1993) 605.
[10] V.K. Gupta, N.B. Pangannaya, World Patent Inform. 22 (2000) 185.
[11] B. Coq, J.M. Planeix, V. Brotons, Appl. Catal. A 173 (1998) 175.
[12] K.P. De Jong, Curr. Opin. Solid State Mater. Sci. 4 (1999) 55.
[13] K.P. De Jong, J.W. Geus, Catal. Rev.-Sci. Eng. 42 (2000) 481.
[14] R.T.K. Baker, N.M. Rodriguez, US Patent 6 485 858 (2000), to Catalytic Materials.
[15] D. Moy, R. Hoch, European Patent 1 176 234 A9 (2002), to Hyperion Catalysis International Inc.
[16] J.E. Fischer, A.T. Johnson, Curr. Opin. Solid State Mater. Sci. 4 (1999) 28.
[17] J.-P. Issi, J.-C. Charlier, in: K. Tanaka, T. Yamabe, K. Fukui (Eds.), The Science and Technology of Carbon Nanotubes, Elsevier, Amsterdam, 1999, p. 107.
[18] C.A. Bessel, K. Laubernds, N.M. Rodriguez, R.T.K. Baker, J. Phys. Chem. 105 (2001) 1115.
[19] D.S. Bethune, C.H. Klang, M.S.D. Vries, J. Gorman, Nature 363 (1993) 605.
[20] M. Ouyang, J.-L. Huang, C.M. Lieber, Acc. Chem. Res. 35 (2002) 1018.
[21] F. Nunzi, F. Mercuri, A. Sgamellotti, N. Re, J. Phys. Chem. B 106 (2002) 10622.
[22] J.-C. Charlier, Acc. Chem. Res. 35 (2002) 1063.
[23] M. Menon, A.N. Andriotis, G.E. Froudakis, Chem. Phys. Lett. 320 (2000) 425.
[24] Q.H. Yang, P.X. Hou, S. Bai, M.Z. Wang, H.M. Cheng, Chem. Phys. Lett. 345 (2001) 18.
[25] S. Inoue, N. Ichikuni, T. Suzuki, T. Uematsu, K. Kaneko, J. Phys. Chem. 102 (1998) 4689.
[26] M. Eswaramoorthy, R. Sen, C.N.R. Rao, Chem. Phys. Lett. 304 (1999) 207.
[27] A. Chambers, C. Park, R.T.K. Baker, N.L. Rodriguez, J. Phys. Chem. 102 (1998) 4253.
[28] J. Hilding, E.A. Grulke, S.B. Sinnott, D. Qian, R. Andrews, M. Jagtoyen, Langmuir 17 (2001) 7540.
[29] K. Masenelli-Varlot, E. McRae, N. Dupont-Pavlosky, Appl. Surf. Sci. 196 (2002) 209.
[30] H. Ulbricht, G. Moos, T. Hertel, Phys. Rev. B 66 (2002) 075404-1.
[31] H. Ulbricht, G. Kriebel, G. Moos, T. Hertel, Chem. Phys. Lett. 363 (2002) 252.
[32] R. Pagani, C&EN 1 (1999) 31.
[33] M.M.J. Treacy, T.W. Ebbesen, J.M. Gibson, Nature 381 (1996) 678.
[34] J. Tang, A. Matsushita, T. Tikegawa, M. Yudusaka, S. Bandow, S. Ijima, Mater. Rec. Soc. Symp. Proc. (2000) 593.
[35] M. Corrias, Ph. Serp, Ph. Kalck, G. Dechambre, J.L. Lacout, C. Castiglioni, Y. Kihn, Carbon, 41 (2003) 2361.
[36] C. Park, R.T.K. Baker, J. Phys. Chem. B 103 (1999) 2453.
[37] J.-M. Moon, K.H. An, Y.H. Lee, Y.S. Park, D.J. Bae, G.-S. Park, J. Phys. Chem. B 105 (2001) 5677.
[38] D. Born, R. Andrews, D. Jacques, J. Anthony, B. Chen, M.S. Meyer, J.P. Selegue, Nano Lett. 2 (6) (2002) 615.
[39] Y. Fan, M. Burghard, K. Kern, Adv. Mater. 14 (2002) 130.
[40] M. Monthioux, Carbon 40 (2002) 1809.
[41] A. Govindaraj, B.C. Satishkumar, M. Nath, C.N.R. Rao, Chem. Mater. 12 (2000) 202.
[42] J.M. Planeix, N. Coustel, B. Coq, V. Brotons, P.S. Kumbhar, R. Dutartre, P. Geneste, P. Bernier, P.M. Ajayan, J. Am. Chem. Soc. 116 (1994) 7935.
[43] Z. Zhong, B. Liu, L. Sun, J. Ding, J. Lin, K.L. Tan, Chem. Phys. Lett. 362 (2002) 135.
[44] P. Chen, X. Wu, K.L. Tan, J. Phys. Chem. B 103 (1999) 4559.
[45] B. Xue, P. Chen, Q. Hong, J. Lin, K.L. Tan, J. Mater. Chem. 11 (2001) 2378.
[46] H.C. Choi, M. Shim, S. Bangsaruntip, H. Dai, J. Am. Chem. Soc. 124 (2002) 9059.
[47] Y. Zhang, N.W. Franklin, R.J. Chen, H. Dai, Chem. Phys. Lett. 331 (2000) 35.
[48] Y. Zhang, H. Dai, Appl. Phys. Lett. 77 (2000) 3015.
[49] X.R. Ye, Y. Lin, C.M. Wai, Chem. Commun. (2003) 642.
[50] A. Chambers, T. Nemes, N.M. Rodriguez, R.T.K. Baker, J. Phys. Chem. B 102 (1998) 2251.
[51] F. Salman, C. Park, R.T.K. Baker, Catal. Today 53 (1999) 385.
[52] K. Otsuka, H. Ogihara, S. Takenaka, Carbon 41 (2003) 223.
[53] R. Gao, C.D. Tan, R.T.K. Baker, Catal. Today 65 (2001) 19.
[54] R.T. K Baker, K. Laubernds, A. Wootsch, Z. Paál, J. Catal. 193 (2000) 165.
[55] N.M. Rodriguez, M.-S. Kim, R.T.K. Baker, J. Phys. Chem. 98 (1994) 13108.
[56] E.S. Steigerwalt, G.A. Deluga, C.M. Lukhart, J. Phys. Chem. B 106 (2002) 760.
[57] R. Vieira, C. Pham-Huu, N. Keller, M.J. Ledoux, Chem. Commun. 954 (2002) 954.
[58] A. Kusnetzova, I. Popova, J.T. Yates, M.J. Bronikowski, C.D. Huffman, J. Liu, R.E. Smalley, H.H. Hwu, J.G. Chen, J. Am. Chem. Soc. 123 (2001) 10699.

[59] T. Kyotani, S. Nakazaki, W.-H. Xu, A. Tomita, Carbon 39 (2001) 771.
[60] T.G. Ros, A.G. van Dillen, J.W. Geus, D.C. Koningsberger, Chem. Eur. J. 5 (2002) 1151.
[61] V. Lordi, N. Yao, J. Wei, Chem. Mater. 13 (2001) 733.
[62] R. Giordano, P. Serp, P. Kalck, Y. Kihn, J. Schreiber, C. Marhic, J.-L. Duvail, Eur. J. Inorg. Chem. (2003) 610.
[63] T.W. Ebbesen, H. Hiura, M.E. Bisher, M.M.J. Treacy, J.L. Shreeve-Keyer, R.C. Haushalter, Adv. Mater. 8 (1996) 155.
[64] Z.-J. Liu, Z.-Y. Yuan, W. Zhou, L.-M. Peng, Z. Xu, Phys. Chem. Chem. Phys. 3 (2001) 2518.
[65] H. Li, J. Ding, J. Chen, C. Xu, B. Wei, J. Liang, D. Wu, Mater. Res. Bull. 37 (2002) 313.
[66] B.C. Satishkumar, E.M. Vogel, A. Govindaraj, C.N.R. Rao, J. Phys. D: Appl. Phys. 29 (1996) 3173.
[67] E. van Steen, F.F. Prinsloo, Catal. Today 71 (2002) 327.
[68] W. Li, C. Liang, J. Qiu, W. Zhu, H. Han, Z. Wei, G. Sun, Q. Xin, Carbon 40 (2002) 787.
[69] S. Hermans, J. Sloan, D.S. Sheppard, B.F.G. Johnson, M.L.H. Green, Chem. Commun. (2002) 276.
[70] C. Park, R.T.K. Baker, J. Phys. Chem. B 102 (1998) 5168.
[71] C. Liang, Z. Li, J. Qiu, C. Li, J. Catal. 211 (2002) 278.
[72] C. Pham-Huu, N. Keller, L.J. Charbonniere, R. Ziessel, M.J. Ledoux, Chem. Commun. (2000) 1871.
[73] C. Pham-Huu, N. Keller, G. Ehret, L.J. Charbonniere, R. Ziessel, M.J. Ledoux, J. Mol. Catal. A: Chem. 170 (2001) 155.
[74] B.L. Mojet, M.S. Hogenraad, A.J. van Dillen, J.W. Geus, D. Koningsberger, Faraday Trans. 93 (1997) 4371.
[75] T.G. Ros, D.E. Keller, A.J. van Dillen, J.W. Geus, D.C. Koningsberger, J. Catal. 211 (2002) 85.
[76] B.C. Satishkumar, A. Govindaraj, G. Mofokeng, G.N. Subbanna, C.N.R. Rao, J. Phys. B: At. Mol. Opt. Phys. 29 (1996) 4925.
[77] X. Lu, F. Tian, Y. Feng, X. Xu, N. Wang, Q. Zhang, Nano Lett. 2 (2002) 1325.
[78] N. Zhang, J. Xie, V.K. Varadan, Smart. Mater. Struct. 11 (2002) 962.
[79] Z. Liu, X. Lin, J.Y. Lee, W. Zhang, M. Han, L.M. Gan, Langmuir 18 (2002) 4054.
[80] S. Banerjee, S.S. Wong, Nano Lett. 2 (2002) 49.
[81] S. Banerjee, S.S. Wong, J. Am. Chem. Soc. 124 (2002) 8940.
[82] Y. Zhang, H.-B. Zhang, G.-D. Lin, P. Chen, Y.-Z. Yuan, K.R. Tsai, Appl. Catal. A: Gen. 187 (1999) 213.
[83] F. Frehill, J.G. Vos, S. Benrezzak, A.A. Koos, Z. Konya, M.G. Ruther, W.J. Blau, A. Fonseca, J.B. Nagy, L.P. Biro, A.I. Minett, M. in het Panhuis, J. Am. Chem. Soc. 124 (2002) 13694.
[84] T.G. Ros, A.J. van Dillen, G.W. Geus, D.C. Koningsberger, Chem. Eur. J. 8 (2002) 2868.
[85] K. Jiang, A. Eitan, L.S. Schadler, P.M. Ajayan, R.W. Siegel, N. Grobert, M. Mayne, M. Reyes-Reyes, H. Terrones, M. Terrones, Nano Lett. 3 (2003) 275.
[86] S. Lee, W.M. Sigmund, Chem. Commun (2003) 780.
[87] M.L. Toebes, F.F. Prinsloo, J.H. Bitter, A.J. Van Dillen, K.P. De Jong, J. Catal. 214 (2003) 78.
[88] M.J. Ledoux, R. Vieira, C. Pham-Huu, N. Keller, J. Catal. 216 (2003) 333.
[89] J.-M. Nhut, R. Vieira, L. Pesant, J.-P. Tessonnier, N. Keller, G. Ehret, C. Pham-Huu, M.J. Ledoux, Catal. Today 76 (2002) 11.
[90] V. Brotons, B. Coq, J.M. Planeix, J. Mol. Catal. 116 (1997) 397.
[91] Z.-J. Liu, Z. Xu, Z.-Y. Yuan, D. Lu, W. Chen, W. Zhou, Catal. Lett. 72 (2001) 203.
[92] C.-B. Li, W.-X. Pan, W.-K. Wong, J.-L. Li, X.-Q. Qiu, X.-P. Chen, J. Mol. Catal. 193 (2003) 71.
[93] H.-B. Chen, J.-D. Lin, Y. Cai, X.-Y. Wang, J. Yi, J. Wang, G. Wei, Y.-Z. Lin, D.W. Liao, Appl. Surf. Sci. 180 (2001) 328.
[94] M.S. Dresselhaus, K.A. Williams, P.C. Eklund, MRS Bull. November (1999) 45.
[95] J.Z. Luo, L.Z. Gao, Y.L. Leung, C.T. Au, Catal. Lett. 66 (2000) 91.
[96] G.G. Kuvshinov, Y.I. Mogilnykh, D.G. Kuvshinov, D.Y. Yermakov, M.A. Yermakova, A.N. Salanov, N.A. Rudina, Carbon 37 (1999) 1239.
[97] V.V. Shinkarev, V.B. Fenelonov, G.G. Kuvshinov, Carbon 41 (2003) 295.
[98] G. Che, B.B. Lakshmi, C.R. Martin, E.R. Fisher, Langmuir 15 (1999) 750.
[99] B. Rajesh, K. Ravindranathan Thampi, J.M. Bonard, N.X. Xanthopoulos, H.J. Mathieu, B. Viswanathan, J. Phys. Chem. B 107 (2003) 2701.
[100] B. Rajesh, V. Karthik, S. Karthikeyan, K. Ravindranathan Thampi, J.M. Bonard, B. Viswanathan, Fuel 81 (2002) 2177.
[101] S.K. Shaikhutdinov, L.B. Avdeeva, B.N. Novgorodov, V.I. Zaikovskii, D.I. Kochubey, Catal. Lett. 47 (1997) 35.
[102] R. Ma, B. Wie, C. Xu, J. Liang, D. Wu, J. Mater. Sci. Lett. 19 (2000) 1929.
[103] C. Pham-Huu, N. Keller, V.V. Roddatis, G. Mestl, R. Schlögl, M.J. Ledoux, Phys. Chem. Chem. Phys. 4 (2002) 514.
[104] K. Hernadi, L. Thien-Nga, E. Ljubovic, L. Forro, Chem. Phys. Lett. 367 (2003) 475.
[105] W. Qian, T. Liu, F. Wei, Z. Wang, H. Yu, Carbon 41 (2003) 848.
[106] C.-H. Li, K-F. Yao, J. Liang, Carbon 41 (2003) 860.
[107] N. Muradov, Catal. Commun. 2 (2001) 89.
[108] G. Mestl, N.I. Maksimova, N. Keller, V.V. Roddatis, R. Schlögl, Angew. Chem. Int. Ed. 40 (2001) 2066.
[109] X. Dong, H.-B. Zhang, G.-D. Lin, Y.-Z. Yuan, K.R. Tsai, Catal. Lett. 85 (2003) 237.